NORGES TEKNISK-NATURVITENSKAPELIGE
UNIVERSITET

Uncertainty in Fault Geometries

by

Hilde G. Borgos and Henning Omre

PREPRINT
STATISTICS NO. 4/2001
ISSN: 0804-9173

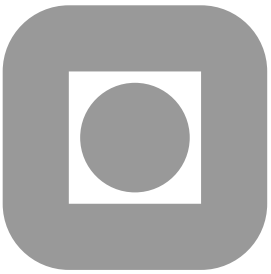

NORWEGIAN UNIVERSITY OF SCIENCE AND
TECHNOLOGY
TRONDHEIM, NORWAY

This report has URL http://www.math.ntnu.no/preprint/statistics/2001/S4-2001.ps
Henning Omre has homepage: http://www.math.ntnu.no/~omre
E-mail: omre@math.ntnu.no
Address: Department of Mathematical Sciences, Norwegian University of Science and Technology,
N-7491 Trondheim, Norway.

Uncertainty in Fault Geometries

Hilde G. Borgos and Henning Omre
Department of Mathematical Sciences, Norwegian University of Science and Technology,
Trondheim, Norway. Email: hgb@stat.ntnu.no, omre@stat.ntnu.no
Ref.: http://www.math.ntnu.no

Abstract

A stochastic model of fault geometries is constructed, enabling fault patterns to be conditioned on available observations from a petroleum reservoir, consisting of three dimensional stacked seismic observations and reflection coefficients obtained from well logs. A Gaussian model is used for the observations, where fault geometries are visible as irregularities in the Gaussian field. The model for fault geometries is defined in a Bayesian framework, where the likelihood model of observations is incorporated together with prior general geological knowledge about fault patterns. Repeated sampling from the model is used to study the uncertainty in fault geometries.

INTRODUCTION

Stochastic modeling of petroleum reservoirs can be used to forecast production, and to assess the associated uncertainty. A model for reservoir characteristics is first defined, based on available observations. A forecast of production is then obtained through a numerical simulation of fluid flow, using the specified recovery procedure. The aim of this work is to define a stochastic model for the fault pattern in a reservoir. The number of faults, their sizes and locations have influence on fluid flow and on the connectivity of the reservoir, and thus on the production forecast.

Two types of information about the fault pattern in a reservoir are available. General geological information about fault characteristics is included in the model. Reservoir specific information provide data on the presence and locations of faults. For example, from seismic observations large faults are detected as discontinuities in the lateral continuity in seismic amplitudes, where the discontinuities are visible throughout a number of subsequent horizontal layers. The stochastic model of fault patterns is constructed in a Bayesian framework, enabling fault patterns to be conditioned on available observations like seismic observations and observations from wells. The uncertainty in fault geometries can be studied through repeated sampling from the posterior stochastic model.

Earlier work on stochastic modeling of faults or fractures include object based techniques, see for example Chilès (1988), and pixel or grid based approaches, e.g., Gringarten (1996). The cited papers present models where observations are used to estimate parameters related to characteristics of fault geometries, while no likelihood function is defined to describe the relationship between fault realizations and available observations. Construction of non-stochastic algorithms for tracking faults from seismic observations was presented by Bahorich and Farmer (1995, 1996), introducing the coherence cube. The coherence cube is a moving window algorithm calculating the correlation between neighbor traces of seismic signals, using local information to reveal discontinuities. The current approach is significantly different from the mentioned publications. A formal stochastic model conditioning on a larger set of seismic traces and well observations is used to assess the uncertainty in the fault pattern.

BAYESIAN FRAMEWORK AND BASIC ASSUMPTIONS

A stochastic model is defined for a faulted horizon H, where the fault pattern is visible as discontinuities in the surface. The aim of this work is to generate geological fault patterns by sampling of the faulted horizon H, conditioned on the available observations, $\boldsymbol{O}$. A Bayesian framework is used to define the relationship between the faulted horizon and the observations. A prior model $f(h)$ of the horizon includes general geological knowledge about faults and fault patterns. The relationship between the faulted horizon and the observations are defined through the likelihood function $f(\boldsymbol{o}|h)$. Combining the prior distribution and the likelihood function, the posterior distribution is obtained,

$$f(h|\boldsymbol{o}) = \text{const} \times f(\boldsymbol{o}|h)\, f(h). \tag{1}$$

The posterior distribution combines general geological knowledge and reservoir specific observations. Assessment of uncertainty in fault geometries is obtained by repeated sampling from the posterior distribution.

In the construction of the stochastic model, some basic assumptions are made. The vertical extents of the faults are assumed to be large compared to the region under study, thus all faults penetrate completely through the vertical extent of the region. Furthermore a crude approximation is made, assuming vertical faults with constant offset within this region.

PRIOR MODEL OF GEOLOGICAL FAULT PATTERNS

In this work post sedimentary faults are considered, and the sedimentary layers of rock are assumed to be originally horizontal. Due to faulting rock is displaced, with a spatial variation in the magnitude of the displacement. As a result, an originally horizontal surface is deformed into a topographic surface in three dimensions, referred to as a horizon. Faults are identified as discontinuities in the horizon. Other natural variations like ductile deformation, folding and tilting are assumed to produce small displacements of the rock compared to the faulting, and result in continuous variations in the altitude of the horizon. Under the assumption of faults penetrating completely through the region under study, the topography of subsequent horizons are comparable. The fault pattern can then be represented by a single horizon H which is given as a topographic map of altitudes $H = H(x, y)$, where the faults, their locations, orientations and offsets, are recognized from the deformations on the surface caused by faulting.

The prior model $f(h)$ of the faulted horizon H includes information of typical characteristics observed in geological fault patterns. For example, information of intersection angles, which are typically close to 60° or 30°, anisotropies in fault orientations and displacement profiles along fault traces are incorporated in the prior model. The faulted horizon is represented by a stochastic gray-scale image based on a hexagonal grid, where both edges, vertices and pixels contain information about the surface, see Figure 1. The hexagonal grid is preferred since it simplifies modeling of intersection angles of 60°. The quantities included in the prior model of a faulted horizon are fault traces on the horizon, offset profiles along the fault traces and the overall topography of the surface.

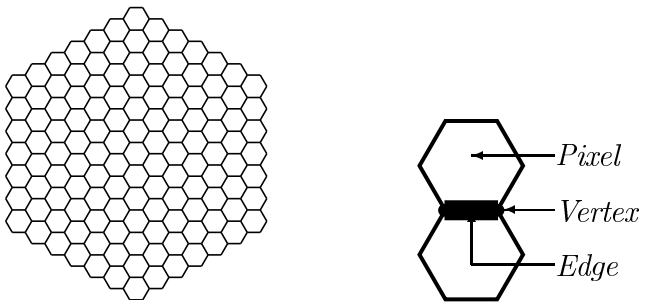

(a) (b)

Figure 1: (a) Hexagonal grid used in the image representation of a faulted horizon. (b) Illustration of an edge (E), vertex (V) and pixel (P) in the hexagonal grid.

The edges $\boldsymbol{E} = (E_1, E_2, \ldots, E_{n_e})$ are binary variables with values $E_i \in \{0, 1\}$, and by connecting edges of value $E_i = 1$ fault traces on the horizon are obtained. Vertices $\boldsymbol{V} = (V_1, V_2, \ldots, V_{n_v})$ are used to model the offsets along the fault traces, their magnitudes and directions, while

vertices off the fault traces are assigned zero value. The pixels $\boldsymbol{P} = (P_1, P_2, \ldots, P_{n_p})$ give the altitude of the horizon H at the center point of each pixel. Altitudes are given in relative coordinates, and does not give an absolute depth. Based on the discrete image representation, the continuous surface $H = H(\boldsymbol{E}, \boldsymbol{V}, \boldsymbol{P})$ is found deterministically by triangulation, accounting for the discontinuities along fault traces. The prior model of the faulted horizon H can be factorized as

$$f(h) = f(\boldsymbol{p}|\boldsymbol{e}, \boldsymbol{v})\, f(\boldsymbol{v}|\boldsymbol{e})\, f(\boldsymbol{e}) \tag{2}$$

where $f(\boldsymbol{e})$, $f(\boldsymbol{v}|\boldsymbol{e})$ and $f(\boldsymbol{p}|\boldsymbol{e}, \boldsymbol{v})$ are prior distributions of edges, vertices and pixels.

A Markov random field is used as a prior distribution of edges, $f(\boldsymbol{e})$. According to the Hammersley-Clifford theorem, see for example Winkler (1995), the distribution of any Markov random field $\boldsymbol{E}$ can be expressed as a Gibbs distribution (Geman and Geman, 1984) with a density function of the form

$$f(\boldsymbol{e}) = \text{const} \times \exp\{-\sum_{c \in \mathcal{C}} \omega_c(\boldsymbol{e}_c)\}. \tag{3}$$

The set $\mathcal{C}$ is the set of all cliques, where a clique is defined as a set of neighboring edges, and $\omega_c(\boldsymbol{e}_c)$ is the potential function of the edges $\boldsymbol{e}_c$ contained in the clique c. The choice of potential functions are inspired by the work of Tjelmeland and Besag (1998). All possible configurations of edges within cliques of size 12 are sorted into specified classes. Figure 2 shows some examples: background, end points, lines, angles and intersections. By assigning different potentials to each class, specific configurations of fault traces are favored. The configurations can also be sorted by direction, giving higher probability to some orientations of fault traces.

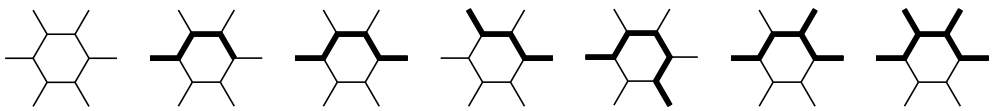

Figure 2: The figure shows some of the classes of clique configurations defined in the prior distribution of edges. (a) A clique where all edges have value $E_i = 0$ is classified as background. Other classes are (b) end point, (c)–(d) lines, (e) angle and (f)–(g) single and double intersection.

The prior model of vertices given edges, $f(\boldsymbol{v}|\boldsymbol{e})$, is a simple model where deterministic offset profiles are assigned to each fault trace. Symmetric offset profiles with a maximum offset near the center of the trace and zero offset at the fault tips are used for isolated fault traces, see for example Dawers, Anders and Scholz (1993). For non-isolated fault traces with fault tips terminating in other fault traces, modifications of the offset profile are made. The number of fault traces and their lengths are determined by the edge values $\boldsymbol{E}$. In our model, only the

direction of the offset is modeled as a stochastic variable, with two possible directions for each fault trace.

A multivariate Gaussian distribution is used as a prior model for the pixels given edges and vertices, $f(\boldsymbol{p}|\boldsymbol{e},\boldsymbol{v})$. The mean vector μ accounts for discontinuities along fault traces. The positions of the fault traces and the magnitude of the offsets depend on the values of $\boldsymbol{E}$ and $\boldsymbol{V}$, thus the mean value μ is given as a function of the edge and vertex values. The prior distribution of pixels is

$$f(\boldsymbol{p}|\boldsymbol{e},\boldsymbol{v}) = \phi(\boldsymbol{p};\mu(\boldsymbol{e},\boldsymbol{v}),\Sigma_p) \tag{4}$$

where $\phi(\boldsymbol{p};\mu,\Sigma)$ is the pdf of the multivariate Gaussian distribution with mean vector μ and covariance matrix Σ. Note that the final offset values along fault traces may differ slightly from the vertex values $\boldsymbol{V}$, and are determined by the difference in pixel values at opposite sides of the fault traces.

LIKELIHOOD MODEL OF RESERVOIR SPECIFIC OBSERVATIONS

Available observations $\boldsymbol{O}$ are included in the model through the likelihood function $f(\boldsymbol{o}|h)$, giving the likelihood of the observations conditioned on the faulted horizon H. Available observations from the reservoir consist of three dimensional seismic data and well logs. An underlying model is defined for reflection coefficients $\boldsymbol{C}$ in three dimensions, and a convolution model is used to model the relationship between reflection coefficients and seismic amplitudes. The observed seismic signals $\boldsymbol{S}^o$ can be expressed as a linear combination of reflection coefficients $\boldsymbol{C}$ and independent Gaussian noise $\boldsymbol{U} \sim N(0,\sigma_s^2 I)$,

$$\boldsymbol{S}^o = A(\psi_s)\boldsymbol{C} + \boldsymbol{U} \tag{5}$$

where $A(\psi_s)$ is a convolution matrix defined by the seismic wavelet with wavelet parameter ψ_s. Based on the well logs, exact observations of reflection coefficients $\boldsymbol{C}^o$ can be obtained at a limited number of locations.

Consider first a sedimentary reservoir prior to any faulting. Reflection coefficients of the reservoir can then be modeled as a Gaussian random field (Eide, Ursin and Omre, 1997; Eide, 1999). From Expression (5) it follows that the seismic signals will then be a Gaussian random field, and the joint distribution of seismic signals and reflection coefficients obtained from well logs can be expressed as a multivariate Gaussian distribution

$$\boldsymbol{O}' \sim N(\mu_o', \Sigma_o') \tag{6}$$

where $\boldsymbol{O}'$ are the observations that would be obtained if gathered prior to faulting. After faulting the original structure of the rock is altered. Recall the model assumptions discussed above, of vertical faults with constant offset and penetrating completely through the vertical extent of the region under study. The fault pattern is represented through the faulted horizon $H(x, y)$. At a point (x, y) the reflection coefficients originally located in (x, y, t) is then displaced to the point $(x, y, t + H(x, y))$, see Figures 3a and 3b. If the faulted horizon $H(x, y)$ is known, observations obtained from the reservoir can be transformed back to their original location, reproducing the initial structure. This is illustrated in Figure 3c.

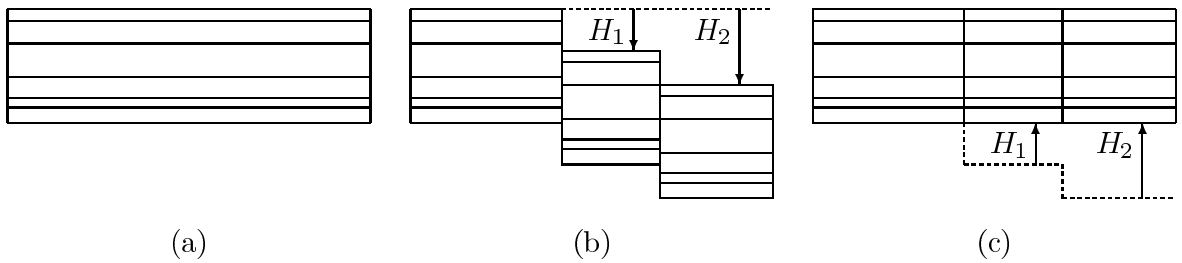

Figure 3: Figure (a) illustrates the structure of the rock prior to faulting. After faulting the structure is altered, as in figure (b). If the faulted horizon H is known, a transformation of observations back to the original structure can be performed, as shown in figure (c).

The position of an observation C^o or S^o gathered from a faulted reservoir does not coincide with the original position prior to faulting. The marginal distributions of the observations are unchanged, but due to the spatial rearrangement the mean vector μ'_o and covariance matrix Σ'_o are no longer valid. The transformation of locations can be expressed as a permutation of the elements of the vector $\boldsymbol{O}'$, giving the observations $\boldsymbol{O}$ of the faulted reservoir, and a corresponding rearrangement of the order of the elements in the mean vector and covariance matrix. The overall distribution of the observations $\boldsymbol{O} = (\boldsymbol{S}^o, \boldsymbol{C}^o)$ is then a Gaussian distribution,

$$[\boldsymbol{O}|H = h] \sim N(\mu_o(h), \Sigma_o(h)) \tag{7}$$

where $\mu_o(h)$ and $\Sigma_o(h)$ are obtained from μ'_o and Σ'_o by rearranging the positions of the elements according to the transformation dictated by the faulted horizon $H = h$. The likelihood function of the observations $\boldsymbol{O}$ is thus the pdf of a multivariate Gaussian distribution:

$$f(\boldsymbol{o}|h) = \phi(\boldsymbol{o}; \mu_o(h), \Sigma_o(h)). \tag{8}$$

SAMPLING FROM THE POSTERIOR MODEL

A posterior distribution $f(h|\boldsymbol{o})$ of the faulted horizon conditioned on available observations is obtained by combining the prior model and the likelihood function. Markov chain Monte Carlo (McMC) techniques are used to generate realizations from the posterior model, see Besag et al.

(1995) and references therein for an introduction to McMC theory. The realizations from the posterior distribution should reflect the discontinuities present in the observations. Not only the position of the discontinuities are located, but also the offsets of the faults. By generating numerous realizations from the posterior model, the uncertainty of the fault pattern in the posterior model can be studied.

The McMC algorithm used to sample from the posterior distribution involves evaluation of the Gaussian likelihood function in Expression (8). The theoretical expression of the likelihood is well known, and can be calculated if the dimension of the observations is small. As the dimension increases however, the likelihood can in practice not be obtained analytically for general Gaussian fields. An approximation to the likelihood function must be found, which in this work consists of two approximations. First, the likelihood function of the observations $\boldsymbol{O}$ is approximated by a pseudo-likelihood function

$$f(\boldsymbol{o}|h) \approx \prod_i f(\boldsymbol{o}_i|\boldsymbol{o}_{-i}, h) \tag{9}$$

where $\boldsymbol{O}_i$ is chosen as a vertical column through the observations, and $\boldsymbol{O}_{-i}$ is the set of all other observations. Next, the conditional distribution is approximated as

$$f(\boldsymbol{o}_i|\boldsymbol{o}_{-i}, h) \approx f(\boldsymbol{o}_i|\boldsymbol{o}_{\partial i}, h) \tag{10}$$

where only observations $\boldsymbol{O}_{\partial i}$ in a neighborhood ∂i of observations $\boldsymbol{O}_i$ are included in the conditioning.

SIMULATION EXAMPLES

The performance of the model presented above is illustrated through simulation examples based on synthetic observations. A three dimensional Gaussian field on a rectangular grid of size $50 \times 50 \times 20$ is first generated, representing the reflection coefficients of the reservoir prior to faulting. Corresponding seismic observations are obtained using the convolution model in Expression (5). Next, a fault pattern and a corresponding faulted horizon are generated from the prior model in Expression (2), see Figure 4, and the resulting structure of the faulted reservoir is found by a rearrangement of the seismic observations, see Figure 5. Hence observations $\boldsymbol{O} = \boldsymbol{S}^o$ of a faulted reservoir are obtained, and samples of the faulted horizon can be generated conditioned on the observations. For these synthetic observations, the true fault pattern and faulted horizon are known, see Figure 4, thus a comparison can be made with the conditional samples.

The hexagonal image representation of the fault pattern covers the lateral extent of the observations, and only the square part of the image where observations are available is illustrated in Figure 4. The image of edges in Figure 4a represents the pattern of fault traces on the surface. The horizon in Figure 4b is discontinuous along the fault traces, with a smooth variation in altitude between faults. The main feature of the fault pattern is two parallel north-west striking faults of opposite dip directions. Figure 4c shows a horizontal cross section through the seismic observations at vertical position $t = 13$, where the faults can be detected as discontinuities in the seismic signals. Figure 5 shows a north-south oriented vertical cross section through the seismic observations at position $x = 25$. Thus the cross section is obtained through the center part of the observations, and crosses the two major faults.

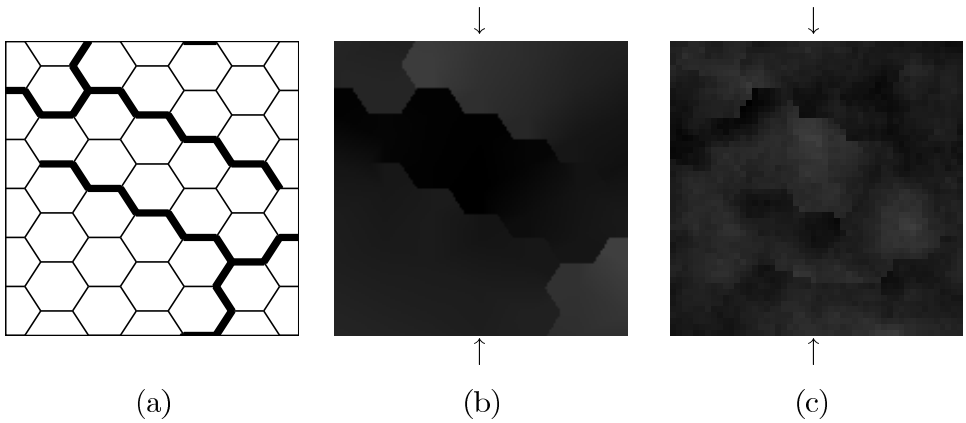

Figure 4: (a) Pattern of fault traces $\boldsymbol{E}$ and (b) faulted horizon H in the square area of observations. The two north-west striking faults are regarded as straight lines, the jagged appearance is an artifact of the hexagonal grid. Figure (c) shows a horizontal cross section through the seismic observations $\boldsymbol{S}^o$, at vertical position $t = 13$, see Figure 5. The arrows mark the position $x = 25$ of the vertical cross section illustrated in Figure 5.

Figure 5: North-south oriented vertical cross section through the seismic observations $\boldsymbol{S}^o$ at position $x = 25$, see Figure 4. The arrows mark the position $t = 13$ of the horizontal cross section in figure 4c.

Figure 6 shows three realizations of the faulted horizon H from the posterior distribution $f(h|\boldsymbol{o})$, based on the synthetic observations described above. The realizations are obtained by performing 50,000 iterations of the McMC sampling algorithm. The algorithm is restarted each time, thus there is no dependency between the realizations. All realizations reproduce the main features of the two dominating faults, while the region near the fault tips differ between the realizations.

Figure 7 shows cross sections of observations corresponding to the cross section in Figure 5, but with observations transformed back to original positions according to the generated faulted horizons in Figure 6. The concept of this transformation is illustrated in Figure 3. After the transformation, the discontinuities produced by the faults should be removed and the original strong horizontal coherence should be retrieved. The fault with the largest offset, to the right in Figure 5, is no longer detectable in the transformed observations based on the two first realizations. In the third realization the offset of this fault is slightly under-represented.

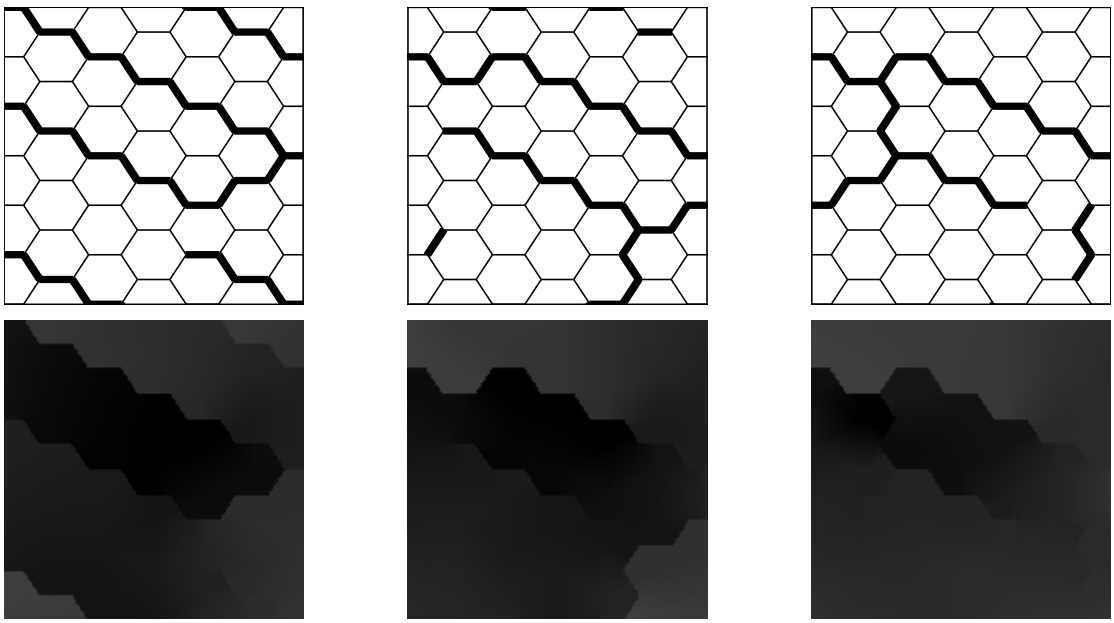

Realization 1 Realization 2 Realization 3

Figure 6: Realizations of pattern of fault traces $\boldsymbol{E}$ (top) and faulted horizon H (bottom) generated from the posterior distribution $f(h|\boldsymbol{o})$ of fault patterns.

CLOSING REMARKS

The paper presents a consistent stochastic model for fault geometries, conditioned to seismic data and well observations, and defined in a Bayesian framework. Through a synthetic data example, it is demonstrated how the stochastic model can be used to assess uncertainties in fault geometry at seismic scales.

Acknowledgments

The authors are grateful to Chris Townsend for giving a basic understanding of the geological aspects related to this problem. We also thank Håkon Tjelmeland for his assistance on this work. H. G. Borgos is funded by a PhD grant from VISTA (*Det Norske Videnskaps-Akademi* and *Statoil*).

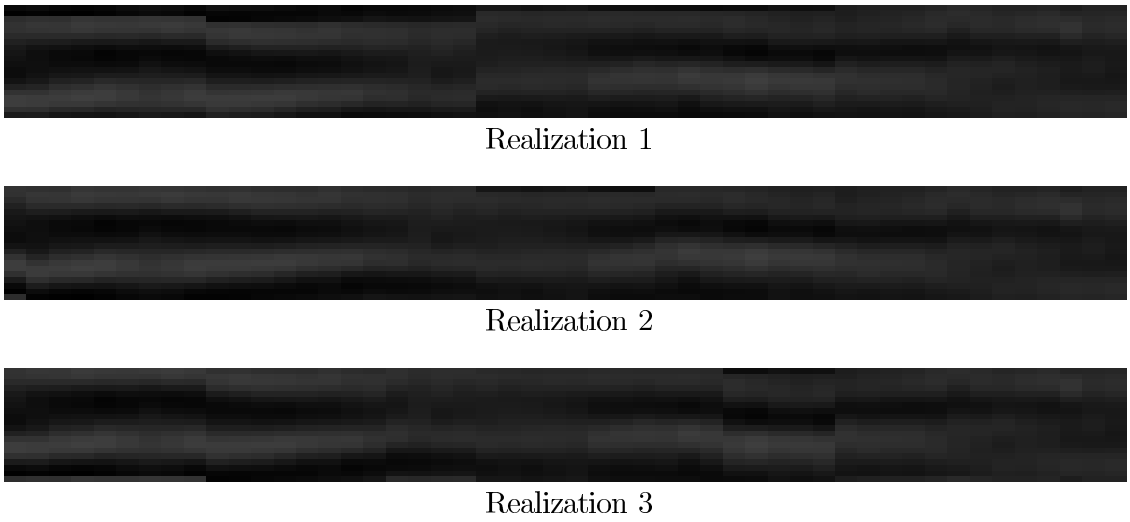

Realization 1

Realization 2

Realization 3

Figure 7: Cross sections corresponding to the section in Figure 5, but with observations transformed according to the generated faulted horizons in Figure 6.

References

Bahorich, M. S. and Farmer, S. L. (1995). The coherence cube, *The Leading Edge* **14**(10): 1053–1058.

Bahorich, M. S. and Farmer, S. L. (1996). Method of seismic signal processing and exploration. U. S. Patent Number 5,563,949.

Besag, J., Green, P., Higdon, D. and Mengersen, K. (1995). Bayesian Computation and Stochastic Systems (with discussion), *Statistical Science* **10**(1): 3–66.

Chilès, J. P. (1988). Fractal and Geostatistical Methods for Modeling of a Fracture Network, *Mathematical Geology* **20**(6): 631–654.

Dawers, N. H., Anders, M. H. and Scholz, C. H. (1993). Growth of normal faults: Displacement-length scaling, *Geology* **21**: 1107–1110.

Eide, A. L. (1999). *Stochastic Reservoir Characterization Constrained by Seismic Data*, PhD thesis, Norwegian University of Science and Technology. Doktoringeniøravhandling 1999:5.

Eide, A. L., Ursin, B. and Omre, H. (1997). Stochastic simulation of porosity and acoustic impedance conditioned to seismic data and well data, *67th Annual Meeting of the Society of Exploration Geophysicists, Expanded Abstracts*, SEG, Dallas, Texas.

Geman, S. and Geman, D. (1984). Stochastic Relaxation, Gibbs Distributions, and the Bayesian Restoration of Images, *IEEE Transactions on Pattern Analysis and Machine Intelligence* **6**(6): 721–741.

Gringarten, E. (1996). 3-D Geometric Description of Fractured Reservoirs, *Mathematical Geology* **28**(7): 881–893.

Tjelmeland, H. and Besag, J. (1998). Markov Random Fields with Higher-Order Interactions, *Scandinavian Journal of Statistics* **25**(3): 415–433.

Winkler, G. (1995). *Image Analysis, Random Fields and Dynamic Monte Carlo Methods*, Springer.